

General Relativistic Radiative Transfer: Applications to Black-Hole Systems

Kinwah Wu¹*, Steven V. Fuerst², Yosuke Mizuno³, Ken-Ichi Nishikawa³, Graziella Branduardi-Raymont¹ and Khee-Gan Lee^{1,4}

¹ Mullard Space Science Laboratory, University College London, Holmbury St Mary, Surrey RH5 6NT, United Kingdom

² Kavli Institute for Particle Astrophysics and Cosmology, Stanford University, Stanford, CA 94304, USA

³ NASA-MSFC/NSSTC, 320 Sparkman Drive, Huntsville, AL 35805, USA

⁴ Department of Astrophysical Sciences, Princeton University, Princeton, NJ 08544, USA

Abstract We present general relativistic radiation transfer formulations which include opacity effects due to absorption, emission and scattering explicitly. We consider a moment expansion for the transfer formulation in the presence of scattering. The formulation is applied to calculations of emissions from accretion and outflows in black-hole systems. Cases with thin accretion disks and accretion tori are considered. Effects, such as emission anisotropy, non-stationary flows and geometrical self-occultation are investigated. Polarisation transfer in curved space-time is discussed qualitatively.

Key words: accretion, accretion disks — black hole physics — galaxies: active — radiative transfer — relativity

1 INTRODUCTION

Observations of the AGN MCG-6-30-15 by *ASCA* showed a Fe $K\alpha$ emission line with a very broad asymmetric profile (Tanaka et al. 1995). The presence of the line was confirmed by later observations using e.g. *Chandra* and *XMM-Newton*. The broad asymmetric Fe $K\alpha$ line has also been seen in the spectra of several other AGN (e.g. NGC 3516, Nandra et al. 1999). The line is believed to be fluorescent emission from accretion flows very close to the black-hole event horizon, where gravitational and kinematic effects are important. There are several mechanisms contributing to the line broadening and profile modification. Rotational motion in the accretion disk causes the line to be double-peaked; relativistic boosting makes the line profile asymmetric – with an enhanced blue (high-energy) line peak and a suppressed red (low-energy) peak; time dilation, due to gravity and transverse relativistic motion, broadens the line and shifts it to a lower energy (see e.g. review by Fabian et al. 2000). Gravitational lensing also distorts the line profile by altering the projection of the emission.

Modeling relativistic lines from black-hole systems has been carried out since the 1970's. In spite of the variations in the numerical/analytic techniques, line-profile calculations generally follow a prescription which can be summarised as follows. (1) Define a space-time metric. (2) Construct a model flat accretion disk to give a macroscopic velocity profile for the emitters. The disk can be stationary or time-dependent, Keplerian or non-Keplerian. Usually a parametric emissivity profile is assumed. Local variations in the disk emission are modeled through parametric prescriptions of turbulence, density/emissivity inhomogeneities, time-dependent flares etc. (3) Determine the geodesics of the “observable” photons and calculate the relative energy shifts of the photons between the emitter and the observer. (4) Bin the photons according to their energies and sum the bins to produce the line spectrum. For time-dependent line profile calculations,

* E-mail: kw@mssl.ucl.ac.uk (kw), sfuerst@stanford.edu (svf)

the photons are also binned and summed according to the arrival time. These calculations have provided us with insights about relativistic effects on line profiles in accreting black holes. However, as observational capabilities improve, we will need more sophisticated radiative transfer calculations so that we can fully utilise the high quality spectral and timing data that the next generation observatories will collect.

2 RADIATIVE TRANSFER FORMULATION

Unless otherwise stated, we use the natural-unit convention ($c = G = \hbar = 1$, where c is the speed of light, G is the gravitational constant, and \hbar is the Planck constant). Without scattering, the general relativistic radiative transfer equation reads

$$\frac{d\mathcal{I}}{d\lambda} = k_\alpha \frac{\partial \mathcal{I}}{\partial x^\alpha} - \Gamma_{\beta\gamma}^\alpha k^\beta k^\gamma \frac{\partial \mathcal{I}}{\partial k^\alpha} = k_\alpha u^\alpha |_\lambda [-\chi_o(x^\beta, \nu)\mathcal{I} + \eta_o(x^\beta, \nu)] \quad (1)$$

(Baschek et al. 1997; Fuerst & Wu 2004; Wu et al. 2006, see also Lindquist 1996), where λ is the affine parameter, $\Gamma_{\beta\gamma}^\alpha$ is the affine connection (determined by the metric $g_{\alpha\beta}$, which is specified by $d\tau^2 = g_{\alpha\beta}dx^\alpha dx^\beta$), k^α is the 4-momentum of photons, and u^α is the 4-velocity of the medium. The Lorentz invariant intensity $\mathcal{I} \equiv I_\nu/\nu^3$, where I_ν is the specific intensity, ν is the frequency, and χ_o and η_o are the Lorentz invariant absorption and emission coefficients respectively. (The subscript ‘‘o’’ denotes that the variable is evaluated at the local rest frame.) In this formulation the radiation is allowed to be self-absorbed internally in the emitting medium, and absorbed and re-emitted in the external line-of-sight media. After the photon geodesics are determined and the emission and absorption coefficients are specified, the radiative transfer equation can be solved along the line-of-sight (Fuerst & Wu 2004), using a ray-tracing algorithm, to determine the emission spectrum.

In the presence of scattering, photons are injected into the line-of-sight from the crossing rays. Equation (1) is therefore inadequate to describe the transfer process. In principle, radiative transfer in a scattering medium must be evaluated globally, instead of by tracing individual rays independently. Obtaining a solution to the corresponding transfer equation is not straightforward and often practically impossible. Various techniques have been developed to bypass the difficulty of direct evaluation of the integro-differential radiative transfer equation. One method is to obtain a solution to a set of differential equations, which provide an acceptable approximation to the exact radiative transfer equation.

For general relativistic radiative transfer in accreting black holes in AGN, the moment method described in Fuerst (2005) is generally applicable. The method may be summarised as follows. First, expand the intensity $\mathcal{I}(x^\alpha, k^\alpha)$ into a series using a set of orthogonal symmetric tensors $J_{\alpha_1 \dots \alpha_j}$, which gives

$$\mathcal{I}(x^\alpha, k^\alpha) = a_0 J + \sum_{i=1}^{\infty} a_i J_{\alpha_1 \alpha_2 \dots \alpha_i} n^{\alpha_1} n^{\alpha_2} \dots n^{\alpha_i}, \quad (2)$$

where n^α is the directional unit vector of the photon. Next, generate a set of projected tensors $\mathcal{J}_{\alpha_1 \alpha_2 \dots \alpha_i \dots}$ satisfying the projection identity

$$\mathcal{P}^{\alpha\beta} \mathcal{J}_{\alpha\beta\gamma_1\gamma_2\dots\gamma_i\dots} = 0, \quad (3)$$

where $\mathcal{P}^{\alpha\beta}$ is the projection tensor perpendicular to u^α , which is a 4-velocity specified in a preferred reference frame, such as the local rest-frame of the medium. We then consider an approximation by truncating the moment expansion. For the j -th order,

$$\mathcal{I}_j(x^\alpha, k^\alpha) = \mathcal{J}_{\alpha_1 \alpha_2 \dots \alpha_j} m^{\alpha_1} m^{\alpha_2} \dots m^{\alpha_j}, \quad (4)$$

where $m^\alpha = n^\alpha + u^\alpha = k^\alpha/E$ (with $E = k^0 \equiv 2\pi\nu$ for the photons). With these, we can derive the moment equations, whose of solutions $\mathcal{J}_{\alpha_1 \alpha_2 \dots \alpha_i}$ form the basis for the construction of various order approximations to the ‘true’ intensity $\mathcal{I}(x^\alpha, k^\alpha)$.

For instance, if the opacity of the medium is contributed by three processes: a free-free process due to a sub-population of thermal electrons (of weight X), synchrotron radiation due to another sub-population

of electrons which is non-thermal (of weight $(1 - X)$), and electron scattering, then the first-order moment equation will be

$$m_\alpha \left[\mathcal{J}^\alpha_{,\beta} n^\beta + \Gamma^\alpha_{\beta\gamma} \mathcal{J}^\gamma m^\beta + \xi \left(\mathcal{J}^\alpha - \frac{\partial \mathcal{J}^\alpha}{\partial (\ln E)} \right) \right] = - [X \sigma_{\text{ff}} + (1 - X) \sigma_{\text{syn}} + \sigma_{\text{T}}] \rho \mathcal{J}^\alpha m_\alpha + X \sigma_{\text{ff}} \rho \mathcal{B} + (1 - X) \sigma_{\text{syn}} \rho \mathcal{S}_{\text{syn}} + \sigma_{\text{T}} \rho \mathcal{J}^\alpha u_\alpha, \quad (5)$$

where $\sigma_{\text{ff},\text{syn},\text{T}}$ are the respective cross sections of the free-free, synchrotron and electron scattering processes, $\mathcal{B} \equiv B_\nu/\nu^3$ is the Lorentz invariant Planck function, and \mathcal{S}_{syn} is the corresponding Lorentz invariant source function for synchrotron radiation. The variable ξ , given by

$$\xi = -\frac{1}{E^2} \frac{DE}{d\lambda} = u^\alpha n_{\alpha;\beta} n^\beta + n^\alpha u_{\alpha;\beta} u^\beta, \quad (6)$$

is a measure of the effective acceleration in the coordinate system – it produces a change in the energy shift as a function of position. If the synchrotron emission is emitted from a population of thermal electrons, then the source function \mathcal{S}_{syn} will be the same as the Planck function \mathcal{B} . Note that the first-order moment equation is analogous to the conventional radiative transfer equation. The first group of terms on the right side correspond to removal of photons by various processes; the next term corresponds to free-free emission; the term after it corresponds to synchrotron emission; the last term corresponds to the injection of photons into the line-of-sight via scattering. The second-order and higher-order equations can be derived accordingly, following similar procedures (Fuerst 2005).

3 THIN RELATIVISTIC ACCRETION DISKS

The radiative transfer formulations presented in Section 2 is applicable to a wide range of astrophysical settings. For calculations of emission from accretion and outflows in black-hole systems. by setting the absorption, emission and scattering coefficient to zero, both formulations easily generate relativistic line profiles as those in Cunningham (1975), Fabian et. al. (1989), Stella (1990), Laor (1991), With the inclusion of the absorption, emission and scattering coefficients, the formulations take full account of the transfer effects.

We will show in the following subsections two applications to geometrically thin accretion disks. The first one concerns angle-dependent effects in the reflection continuum. The second concerns a more complex situation, in which the emitting and absorbing media vary with time, and emission and absorption are not confined to the disk equatorial plane. Hence, angle-dependent emission and absorption must be treated explicitly throughout the entire region.

3.1 Angle-dependent Emission – Reflection Spectra

An AGN X-ray emission spectrum generally consists of a soft thermal black-body component, a hard power-law component, and a reflection component including the lines, e.g. the fluorescent Fe $K\alpha$ line. The thermal black-body, the power-law component and the lines are probably isotropic. The reflection component, however, depends strongly on the viewing angle. In the analyses of X-ray spectra, model fits to the reflection component often assume a fix viewing angle, chosen to be the same as the viewing inclination of the normal of a geometrically thin accretion disk. This assumption can be problematic, as the space-time in the inner accretion disk is curved and the emission is gravitationally lensed. The pitch angles of the photons from a disk surface element that reach a distant observer are not the same as the inclination angle specifying the orientation of the accretion disk. Light aberration is also non-negligible as the flows in the inner accretion disk are highly relativistic. The situation is further complicated by the rotation of the black hole, which leads to reference frame dragging. Moreover, limb effects occur when the emission emerges from the disk surface. (See Lee et al. (2007) and Wu et al. (2006).)

Gravitational and relativistic kinematic effects coupled with anisotropic reflection will lead to a number of observable consequences. Figure 1 illustrates some of the consequences by (i) a comparison between a relativistic disk reflection spectrum and a rest-frame spectrum (where the reflection spectra comprise only a continuum and absorption edges), and (ii) a comparison between reflection spectra from accretion disks around black holes with different spin parameters. The first demonstrates how local angle-dependence

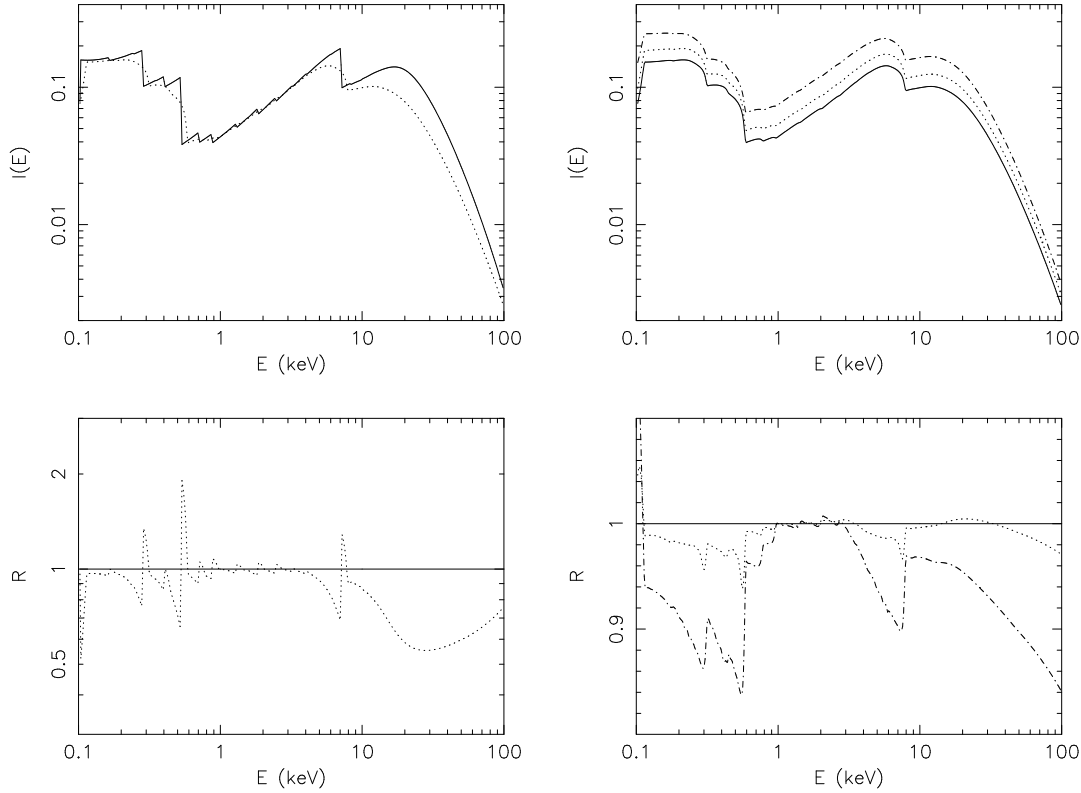


Fig. 1 The upper left panel shows the comparison between a reflection spectrum of a geometrically thin relativistic accretion disk around a Schwarzschild black hole (dotted line) and a rest-frame reflection spectrum (solid line) generated by PEXRAV in XSPEC based on the model calculation of Magdziarz & Zdziarski (1995). The viewing inclination angle of the disk is 45° . The local intensity of the emission from the disk surface follows a radial power-law profile with an index of -2 . The bottom left panel shows the corresponding quotient spectra, which are obtained by dividing the spectra by the rest-frame spectrum. The upper right panel shows reflection spectra of thin accretion disks around black holes with spin parameters $a = 0, 0.5$ and 0.998 (solid, dotted and dot-dashed lines respectively). The bottom right panel shows the corresponding quotient spectra, which are obtained by dividing the spectra by the spectrum of the case with $a = 0$. In all the reflection spectra the intensity $I(E)$ is in an arbitrary unit. The quotient spectra are normalised, such that the normalised intensity $R = 1$ at energy $E = 1$ keV.

together with relativistic energy shift modifies the reflection continuum. The second shows how the effects combine with the rotation of the black hole, giving rise to broad features mimicking relativistic emission lines.

One obvious difference between a relativistic reflection spectrum and a rest-frame spectrum is the smearing of the absorption edges. The quotient spectra in Figure 1 imply that fitting the reflection spectrum of a relativistic accretion disk using model rest-frame reflection spectra will result in a flux excess blue-ward of the edge and a flux deficiency red-ward of the edge. These may lead to an artifact resembling a blue-shifted emission line, which has a wavelength consistent with the element species associated with the edge. The artifact feature may also be mistaken as an emission line from relativistic outflows. Another obvious difference is in the $10 - 100$ keV spectral region. The reflection peak is lowered and the high-energy tail is flattened in the relativistic spectrum. These will affect the slope of the fit power-law for the observed

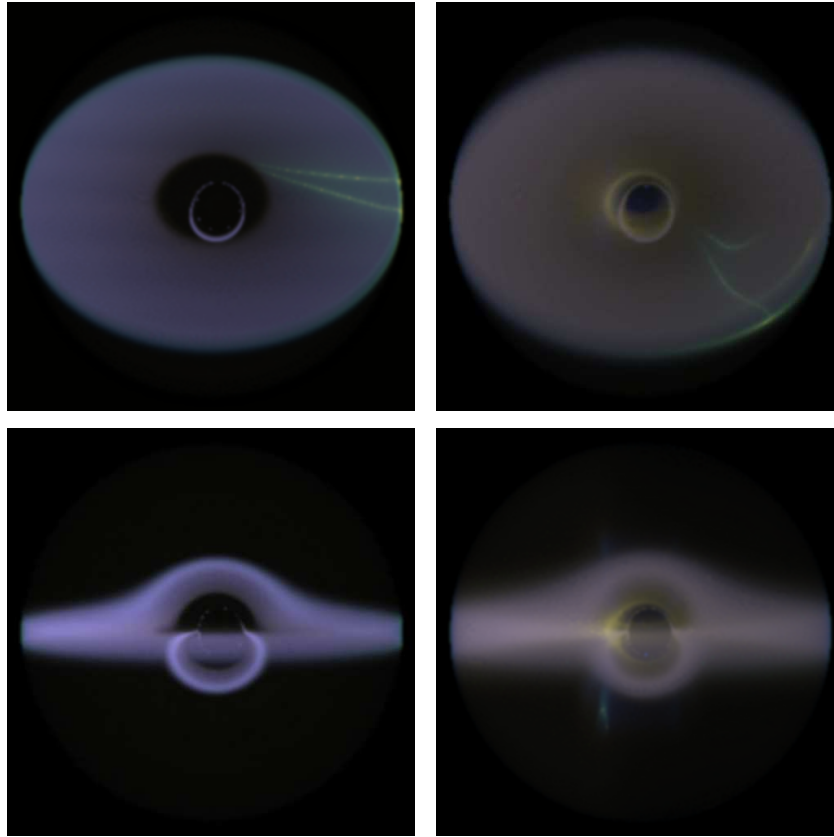


Fig. 2 The panels on the top row show images of emissions from the flows, viewed at an inclination angle of 45° , at time $t/\tau_s = 0$ (left) and 300 (right) (where $\tau_s = r_s/c$, and r_s is the Schwarzschild radius of the black hole), corresponding to an initial state and a later state of the simulation. Bright synchrotron filaments (in greenish blue colour) are seen near the disk surface. The bright blue ring at the center is the first-order lensed disk image. The fuzzy yellowish ring near the center in the image at $t/\tau_s = 300$ is due to direct thermal free-free emission from dense material piled up in the inner accretion disk. The panels on the bottom row show images of emissions from flows viewed at an inclination angle of 85° for $t/\tau_s = 0$ (left) and 300 (right). The faint vertical features below the disk are the components of the counterpart jet.

spectrum. The effect is severe in situations where the spectral coverage at the high-energies, say above 20 keV, is unavailable.

The effects of the black hole's rotation on the reflection spectra of relativistic disks are manifested predominantly in the red-ward region of the absorption edge (panels in the right column, Fig. 1). The disk reflection spectrum of a fast rotating black hole shows a flux deficiency red-ward of the edge compared to the disk reflection spectrum of a slower rotating black hole. Using spectral models corresponding to fast-rotating black holes in fits to the spectral data of a system with a slowly rotating black hole will therefore yield a flux excess red-ward of the edge. The flux excess may appear as a line-like feature with a profile resembling those of relativistic emission lines for Schwarzschild black holes or even fast rotating Kerr black holes, depending on the relative rotational rate of the two black holes in the comparison. The high-energy tail of the reflection spectrum is also affected by the black-hole spin. The general trend is that the more rapidly the black hole rotates, the steeper the slope of the high-energy spectral tail.

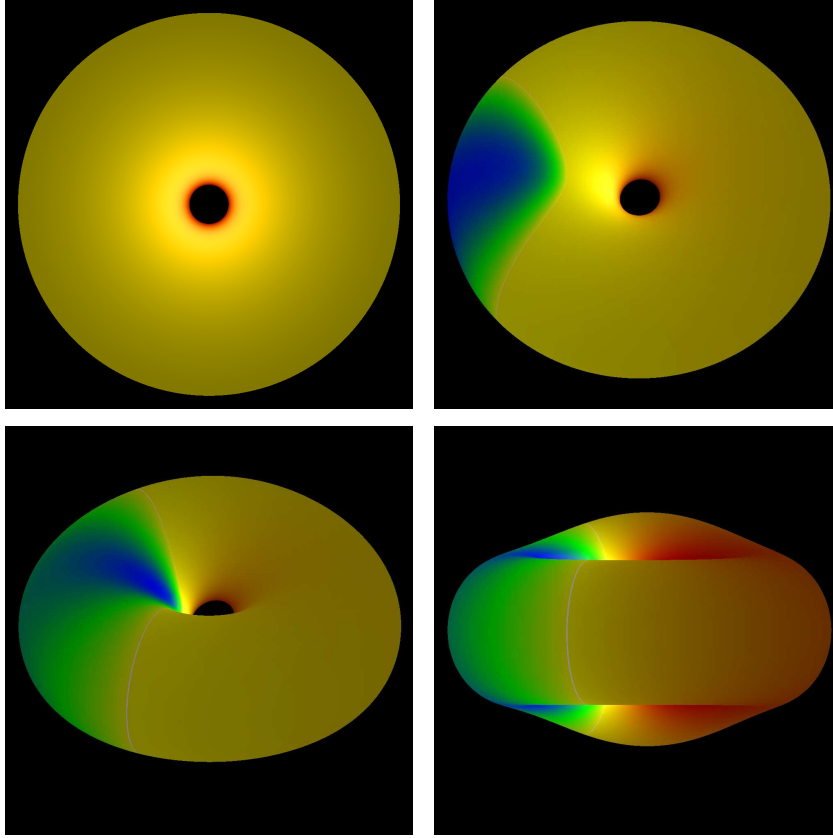


Fig. 3 Energy shift images of opaque relativistic accretion tori around a rotating black hole with a spin parameter $a = 0.998$, viewed at inclination angles $i = 1^\circ, 30^\circ, 60^\circ$ and 89° (panels ordered from left to right and top to bottom). Red indicates red shifts in energy and blue, blue shifts. The tori have a rotational velocity profile index $n = 0.1$ (see Fuerst & Wu 2007) and the innermost boundary of the emission surface reaches $1.3 r_g$, where the gravitation radius $r_g = 1$ for normalised black-hole mass.

Note that the change of the emission spectrum with the viewing inclination of a system is not restricted to the case of photon pitch-angle isotropy with respect to the normals of the emission surface elements. It also occurs when the emission or absorption of the line-of-sight material is anisotropic, e.g. a medium permeated by a magnetic field.

3.2 Time-varying Accretion and Magnetised Outflow

The current time-dependent calculations of emission from relativistic flows are mostly focused on effects of dynamics. Generally, these calculations employ a generic ray-tracing algorithm and ignore all the opacity effects in the emitting and transmitting media. Although these studies have provided some useful insights on how space-time curvature and relativistic kinematics modify the spectrum shape, they fail to provide a direct diagnostic to the spectral formation in accreting black holes. For instance, to calculate the emission from a relativistic accretion disk with a dense magnetised outflow, one needs to treat emission and absorption explicitly, in addition to space-time curvature and other relativistic effects.

Magnetised accretion disks and outflows are known to be non-steady. The magnetic fields embedded in the flows are twisted continually, and the local field strengths fluctuate. The rapid variations in the field configuration and in the flow coupled with gravitational lensing give rise to a number of unexpected phe-

nomena. Figure 2 shows the emission from a simulated flat accretion disk and its outflow. The size of the region is about ten Schwarzschild radii, where general relativistic effects are significant. The dynamical variables are obtained by a 2.5-D general relativistic MHD simulation using the 3-D RAISHIN code (Mizuno et al. 2006a,b). In the radiative transfer calculations the opacity is assumed to be due to thermal free-free and synchrotron processes. Bright filament-like features appear in the disk image. They are caused by chance alignment of magnetic field lines, along which the electrons are streaming in relativistic speeds. Synchrotron radiation from these fast streaming electrons is beamed and boosted. As the simulation evolves, the bright features wiggle quasi-periodically (i.e. QPOs), on time scales of the order that of the local flow dynamics. These bright filament-like features are robust — seen at all viewing inclinations. They are geometrical in nature, and are therefore not sheared by the differential rotation of the accretion disk. This is in contrast to material clumps circulating around in the accretion disk, which disperse after a few orbits.

The simulation shows the development of a pair of jets in the outflows. The counter-jet below the equatorial plane is more visible (see the bright features protruding from the disk in Fig. 2). There are two concentric components in each jet. They have different dynamical and emission properties. The simulation also shows material pile-up in the inner disk, which gives rise to strong free-free emission.

4 RELATIVISTIC ACCRETION TORI

4.1 Opaque Tori

An accretion torus is a 3-D object, unlike a geometrically thin accretion disk, which is 2-D. Several methods commonly used in relativistic line calculations for thin accretion disks around black holes (e.g. Cunningham 1975) are inapplicable to accretion tori, as in this case the emission originates from surfaces outside the equatorial plane. The situation is further complicated if the emission is angle dependent. While the entire upper surface of a geometrically thin accretion disk is always visible, self-occultation effects in tori are important at high viewing inclination angles (Fig. 3). This plays a very significant role in shaping the emission line profiles. Figure 4 shows the profiles of emission lines from two accretion tori with different thicknesses (specified by the velocity profile parameter, n , see Fuerst & Wu 2007) viewed at various inclination angles. The torus with $n = 0.1$ has substantial thickness (see Fig. 3); the torus with $n = 0.001$ is practically the same as a geometrically thin disk. Both tori show similar line profiles at low inclination angles. The lines are red-shifted because of gravitational red-shift and transverse Doppler effect. The differences between lines from the two tori become more visible for viewing inclinations i larger than $\sim 45^\circ$. At high inclination angles, lines from tori with larger n are narrower, i.e. suffer less red-shift and less blue-shift, as the innermost region, where relativistic effects are most severe, is self-occulted. This demonstrates that extracting information about the system parameters is non-trivial, as geometrical factors (such as aspect ratio of the accretion torus/disk) could affect the maximum red-shift and the maximum blue-shift in the line profile, confusing the estimation of the location of the last stable particle orbit and hence the spin of the central black hole.

4.2 Semi-transparent Tori

Another difference between an accretion torus and an accretion disk is that the emission is not restricted to a surface when the torus is not opaque. The entire accretion torus contributes to the emission seen by the distant observer (Fig. 5). The relativistic beaming is more important than for the opaque tori, where the most beamed/boosted emission is hidden because of self-occultation. If the torus is semi-opaque, then various complicated opacity effects may occur. For example, if two lines differ slightly in wavelengths, the line emitted from one part of the torus may resonate with the other line from another part of the torus, because of energy shifts due to velocity shears and the difference in the gravitational potentials between the emitters and the line-of-sight absorber/scatterers. While the emission lines from such tori are still broad and asymmetric as those of the opaque disks and tori, the line profiles are not identical (Fuerst 2005).

4.3 Scattering Dominated Tori

In a scattering torus, the opacity is provided by electron scattering as well as line/continuum absorption. As photons can be scattered into a ray from a cross ray, the radiative transfer needs to be evaluated globally. With the moment formulation described in Section 2, the emission from scattering tori can be calculated, and Figure 6 shows an example. Although a scattering torus may resemble a semi-transparent absorptive

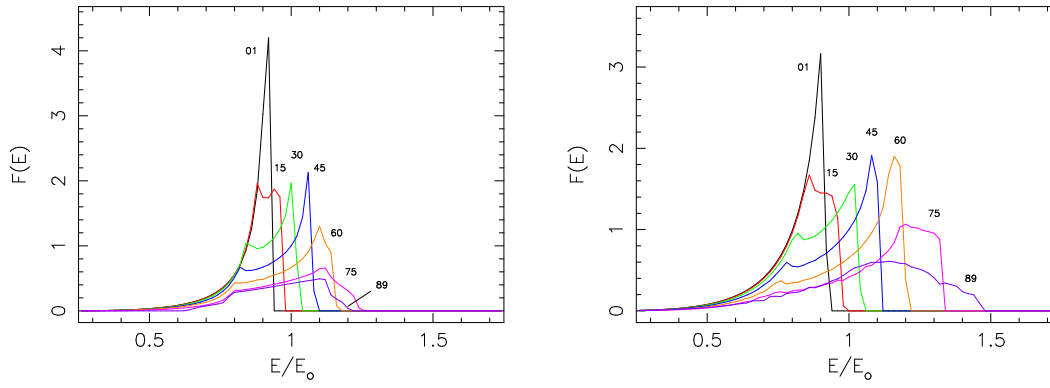


Fig. 4 The left panel shows the emission line profiles of an opaque torus with the same parameters as those in Fig. 3 (i.e. $n = 0.100$), viewed at inclination angles of $i = 1^\circ, 15^\circ, 30^\circ, 45^\circ, 60^\circ, 75^\circ$ and 89° . The right panel shows the emission line profiles of an opaque torus with parameters the same as those of the torus in the left panel except that $n = 0.001$ (i.e. practically a thin disk). The intensity $I(E)$ is normalised such that $I(E) = 1$ at $E/E_0 = 1$ for $i = 45^\circ$.

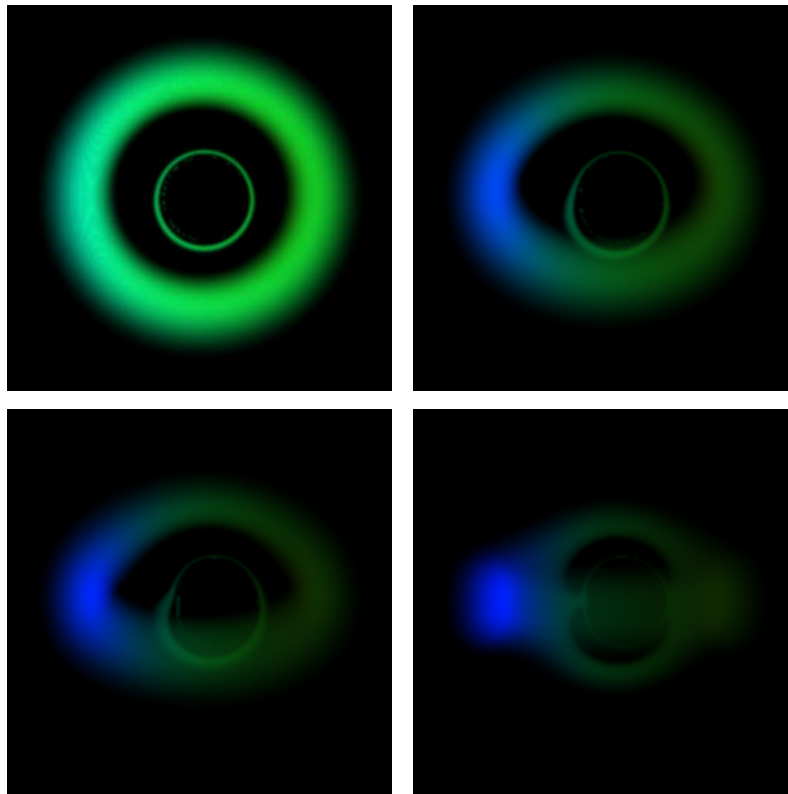


Fig. 5 Surface brightness of semi-transparent accretion tori around black holes with $a = 0.998$, viewed at inclinations $i = 15^\circ, 45^\circ, 60^\circ$ and 85° (panels from left to right and from top to bottom). The opacity is due to the opacities of the Fe $K\alpha$ and $K\beta$ lines. The brightness is normalised such that the maximum pixel brightnesses of all tori in the images are the same.

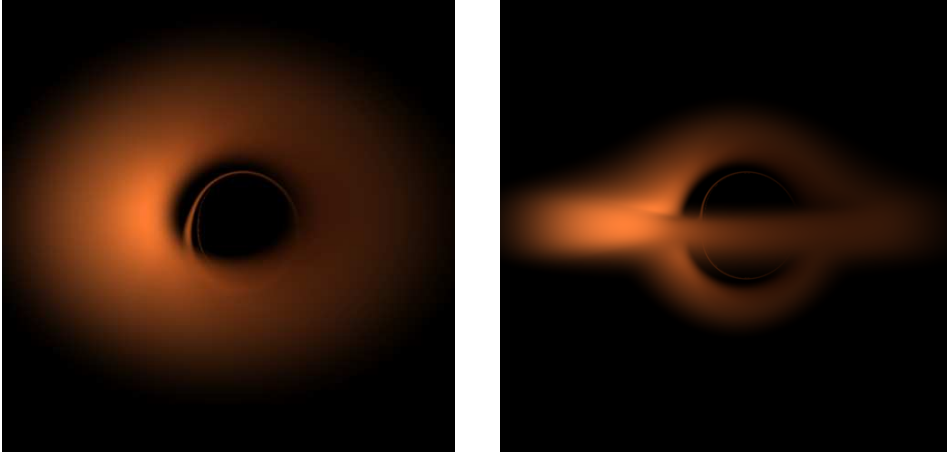


Fig. 6 Surface brightness of scattering accretion tori around black holes with $a = 0.998$, viewed at inclinations $i = 45^\circ$ (left) and 85° (right). The opacity is due to electron scattering. The brightness is normalised such that the maximum pixel brightnesses of the two tori are the same.

torus in appearance, their emission properties are very different. Firstly, line resonance has difficult to occur in a strongly scattering torus. Secondly, the beaming effects are less obvious in a torus with electron scattering, as the beamed emission can be scattered out of the line-of-sight. This is in strong contrast to an absorptive torus, where a beamed line photon is up-shifted in energy so that it will not suffer resonant scattering/absorption. The total emission from an opaque torus is the sum of weighted and shifted Planck functions from the visible torus surface elements. This is not true for a scattering thick torus: the scattered emission is not necessarily thermal and its total emission is not simply a sum of the weighted and shifted local Planck functions of the visible elements on the last scattering surface. In addition to all these, a scattering thick torus is expected to show strong polarisation, but the emission from an opaque absorptive torus would be unpolarised.

5 BRIEF COMMENTS ON POLARISED RADIATIVE TRANSFER

In Newtonian space-time, the polarised radiative transfer equation may be expressed as

$$\hat{D} I_i(\nu, \hat{\Omega}) = -K_{ij} I_j(\nu, \hat{\Omega}) + j_i(\nu, \hat{\Omega}) + \int d\nu' \int d\hat{\Omega}' S_{ij}(\nu, \nu'; \hat{\Omega}, \hat{\Omega}') I_j(\nu', \hat{\Omega}'), \quad (7)$$

where i and j are indices for the polarisation modes, I_i is the intensity of a polarisation mode, j_i is the emission coefficient, K_{ij} is the opacity, whose diagonal elements specify absorption of the polarisation and off-diagonal elements specific polarisation conversion and rotation, S_{ij} is the scattering matrix, and $\hat{\Omega}$ is the directional unit vector of the radiation propagation. The propagation differential operator is given by

$$\hat{D} \equiv \frac{1}{c} \frac{\partial}{\partial t} + \hat{\Omega} \cdot \nabla. \quad (8)$$

Equation (7) implies that the creation of a polarisation mode and the conversion between different polarisation modes are caused by the media, either the emitters or the line-of-sight material. For instance, in the presence of a magnetic field, gyrating electrons will give rise to cyclotron and synchrotron radiations, which are polarised. The polarisation will undergo Faraday rotation/conversion when the radiation propagates in a magnetised plasma (Fig. 7). Scattering may also induce polarisation. The propagation operator, however, does not affect the polarisation properties of the radiation. In curved space-time, this may not be true – 3-vectors defined on a local Lorentzian space-time are not preserved undergoing parallel transport

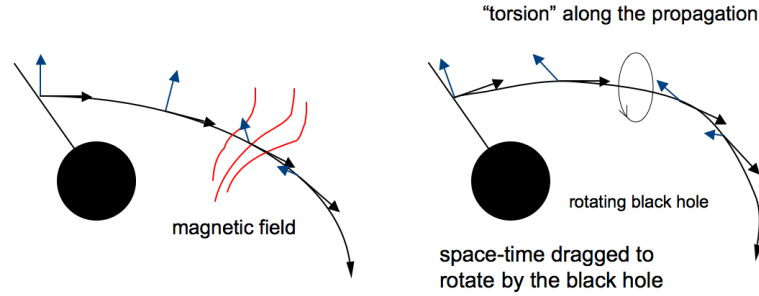


Fig. 7 Schematic illustrations showing the rotation of polarisation vectors in the presence of magnetic field (left) and in rotational space-time (right) as the radiation propagates.

along a geodesic (see e.g. Misner, Thorne & Wheeler 1973). The orientations and strengths of the electric and magnetic fields (seen by a distant observer) change as the radiation propagates in a curved space-time, resulting in rotation, stretching and twisting of the polarisation vectors. If the space-time is rotating, such as that around a Kerr black hole, the polarisation vectors can also be dragged into rotation (Fig. 7). For radiative transfer in black-hole environments, conversion and rotation of the polarisation vectors are caused by space-time curvature and rotation as well as by the radiative properties of the emitters and the transmitting media. To disentangle all these effects is non-trivial. However, before this difficult task can be carried out, one needs to have a fully covariant polarisation radiative transfer formulation applicable to and suitable for astrophysical settings, which is currently lacking.

6 SUMMARY

We present a general relativistic formulation for radiative transfer which treats emission and absorption processes explicitly. We also present a more general formulation which includes scattering in addition to emission and absorption. A moment solution is derived for this equation. The formulations are applicable to calculate the emission from accretion disks and accretion tori around black holes. Cases of reflective flat disks, opaque tori, semi-transparent tori and scattering tori are presented to illustrate various effects, which conventional ray-tracing relativistic line calculations have failed to recognise. Polarisation transfer in curved space-time is briefly discussed.

We summarise our findings as follows. (1) Angle-dependent effects are important, and improper modeling of the reflection continuum will give rise to artifact features with profiles very similar to those of relativistic lines from accretion disks around fast rotating black holes. (2) Time dependent flows in the presence of magnetic fields together with relativistic beaming can give rise to QPOs in the emission. (3) Self-occultation is important for opaque accretion disks with substantial thickness (i.e. accretion tori) at high viewing inclination angles. Lines from the thicker tori are narrower and show less relativistic effects, as emission from the inner surface, where the gravitational field is the strongest and the flow is the faster, is obscured. (3) Emission from semi-transparent accretion tori show more relativistic beaming effects. Processes forbidden in opaque disks/tori, such as resonance of lines with different wavelengths, can occur in semi-transparent disks, due to gravitational potential gradients and velocity shear. (4) Opaque scattering tori and opaque absorptive tori have different radiative properties, and an opaque scattering torus does not necessarily have a thermal spectrum which is the sum of weighted Planck functions shifted in energies.

Acknowledgements We thank Curtis Saxton and Roberto Soria for the comments on the manuscript.

References

- Baschek B., Efimov G. V., von Waldenfels W., Wehrse R., 1997, *A&A*, 317, 630
Cunningham C. T., 1975, *ApJ*, 202, 788
Fabian A. C., Rees M. J., Stella L., White N. E., 1989, *MNRAS*, 238, 729
Fabian A. C., Iwasawa K., Reynolds C. S., Young A. J., 2000, *PASP*, 112, 1145
Fuerst S. V., 2005, PhD Thesis, University of London
Fuerst S. V., Wu K., 2004, *A&A*, 424, 733
Fuerst S. V., Wu K., 2007, *A&A*, submitted
Laor A., 1991, *ApJ*, 376, 90
Lee K.-G., Fuerst S. V., Branduardi-Raymont G., Wu K., Crowley O., 2007, *PASA*, submitted
Lindquist R., 1996, *Annals of Physics*, 37, 487
Magdziarz P., Zdziarski A. A., 1995, *MNRAS*, 273, 387
Misner C. W., Thorne K. S., Wheeler J. A., 1973, *Gravitation*, San Francisco: W H Freeman
Mizuno Y., Nishikawa K. I., Koide S., Hardee P., Fishman G. J., 2006a, *ApJS*, submitted (astro-ph/0609004)
Mizuno Y., Nishikawa K. I., Koide S., Hardee P., Fishman G. J., 2006b, *ApJ*, submitted (astro-ph/0609344)
Nandra K., George I. M., Mushotzky R. F., Turner T. J., Yaqoob T., 1999, *ApJ*, 523, L17
Stella L., 1990, *Nature*, 344, 741
Tanaka Y. et al., 1995, *Nature*, 375, 659
Wu K., Fuerst S. V., Lee K.-G., Branduardi-Raymont G., 2006, *Chin. J. Astron. Astrophys. (ChJAA)*, 6S1, 205

DISCUSSION

JAMES BEALL: Two questions: (1) In the rest frame of the plasma the electrostatic instability (for a jet with multiple velocities) is very fast. Do you have an idea of its growth time in the frame of the observer? (2) You have used both the Kerr metric and the Schwarzschild metric to calculate the emission. What parameters did you take for the Kerr metric?

KINWAH WU: I do not have the values for the growth timescales of the instabilities. However, if allowing me to make a guess, I would say it is of the order of the dynamical timescale of the system. The flows are relativistic and it occurs near the black hole. A natural choice would be the Schwarzschild radius of the black hole divided by the velocity light. As for the parameter of the Kerr black hole in the calculations, we used a range of black-hole spin parameter from 0 to 0.998. In this presentation I showed the results of the very extreme case with $a = 0.998$ (unless otherwise stated). This is for the purpose of illustrating the contrast between a non-rotating black hole and a very rapidly rotating black hole. Our calculations were not restricted to the extreme situations.

WOLFGANG KUNDT's Comment: I appreciate the highly non-trivial effort your colleagues and you have taken to derive manageable expressions for realistic radiative transfer from black hole accretion flows. But, as you know, an additional complication of their application to concrete sources can be additional trans-relativistic motions in and beyond the BLR of AGN.